Li, X., Hallett, S. R., & Wisnom, M. R. (2015). Modelling the effect of gaps and overlaps in automated fibre placement (AFP)-manufactured laminates. Science and Engineering of Composite Materials, 22(2), 115-129. DOI: 10.1515/secm-2013-0322

Peer reviewed version

Link to published version (if available):
10.1515/secm-2013-0322

Link to publication record in Explore Bristol Research
PDF-document

This is the author accepted manuscript (AAM). The final published version (version of record) is available online via De Gruyter at http://www.degruyter.com/view/j/secm.2015.22.issue-2/secm-2013-0322/secm-2013-0322.xml. Please refer to any applicable terms of use of the publisher.

University of Bristol - Explore Bristol Research

General rights

This document is made available in accordance with publisher policies. Please cite only the published version using the reference above. Full terms of use are available:
http://www.bristol.ac.uk/pure/about/ebr-terms.html

Published in Science and Engineering of Composite Materials 2015; 22(2): 115–129
DOI 10.1515/secm-2013-0322

Modelling the effect of Gaps and Overlaps in Automated Fibre Placement (AFP) manufactured laminates

X. Li, S. R. Hallett and M. R. Wisnom

Advanced Composites Centre for Innovation and Science, University of Bristol,

Queens Building, University Walk, Bristol, BS8 1TR

(xq.li@bristol.ac.uk)

Abstract: In Automated Fibre placement (AFP) process, gaps and overlaps parallel to the fibre direction can be introduced between the adjoining tapes. These gaps and overlaps can cause a reduction in strength as compared with pristine conditions. Finite element modelling is an effective way to understand how the size and distribution of such gaps and overlaps influences the strength and failure development. Many modelling work showed that out-of-plane waviness and ply thickness variations caused by gaps and overlaps play an important role in inducing the strength knock-down, however there has been a lack of effective way to explicitly model the ply waviness, which constrained the relevant research. In this work 3D meshing tools were developed to automatically generate ply-by-ply models with gaps and overlaps. Intra-ply and inter-ply cohesive elements are also automatically inserted in the model to capture the influence of splitting and delamination. Out-of-plane waviness and ply thickness variations caused by gaps and overlaps are automatically modeled. Models with various sizes and distribution of gaps and overlaps were built to predict the reduction of strength as a function of the magnitude and type of the defects. Results of gap and overlap models will be used to guide future experimental characterization of simulated AFP process defects, manufactured by hand layup from pre-preg tape.

Keywords: *automated fibre placement, defects, gaps, overlaps, failure*

Published in Science and Engineering of Composite Materials 2015; 22(2): 115–129
DOI 10.1515/secm-2013-0322

1 Introduction

The Automated Fibre Placement (AFP) process shows great potential for efficient manufacturing of large composite structures. An AFP machine consists of a computer controlled robotic arm with a placement head (refer to Fig. 1) that lays bands of pre-preg strips (slit tape) onto a mould in order to construct the layup. The pre-preg strips are relatively narrow (~6mm wide tapes). Due to the complexity of the tape laying process, gaps and overlaps parallel to the fibre direction, as shown in Fig. 2, can be introduced between adjoining tapes. These gaps and overlaps can cause a reduction in strength as compared with pristine conditions. It is important to understand how the size and distribution of such gaps and overlaps influences the strength and failure development. Some experimental work has been done to study the effects of gaps and overlaps. For instance, Sawicki and Minguet [2] explored the effect of aligned and isolated gaps in 90° plies in a compression strength test, Turoski [3] systematically studied the effects of isolated gaps and interacting gaps with different stagger repeats on the strength of unnotched and notched quasi-isotropic laminates in both tension and compression tests. Croft et al [4] have investigated the influence of a gap, an overlap and a half gap/overlap located at the through-thickness symmetry plane in a laminate by tension, compression and in-plane shear tests. These works provide very informative results, however compared with the large number of different and complex combinations and permutations for gap and overlap defect types in aerospace structures, they represent only a small sub-set of the possible configurations that can occur. The range of defect parameters such as the tow width, defect size, defect stagger repeat and stagger distance would require a very large test plan to fully evaluate the full range of failure mechanisms and strengths. Finite element modeling is a comparatively more effective way to understand the interactions of these defects and provide guidelines on the tolerance of gaps and overlaps. Researchers have used various finite element methods to understand failure mechanisms caused by gaps and overlaps in composites. Cairns et al [5] used local inhomogeneity models with double stiffness for overlap regions and resin properties for gaps to study the influence of defects on the tensile failure. They found that the sub-critical damage like splits and delamination played a greater role than the inhomogeneity in its influence on the failure. Sawicki and Minguet [2] modeled gaps and overlaps by varying the thickness of 90° plies locally (gaps were not explicitly modeled as resin pockets) to capture the out-of-plane waviness caused by gaps and overlaps. They concluded that the waviness

appeared to induce failure mechanisms that reduced the laminate compression strength. Turoski [3] used similar methods to Cairns in modeling the gaps, using the resin properties for gaps and ignoring the influence of out-of-plane waviness and sub-critical damage. This work suggested that much of the strength reduction comes from the geometry perturbations that gaps induce; out-of-plane waviness and thickness variations. Lopes, Gürdal and Camanho [6,7,8] studied the influence of triangular gaps and overlaps at the tow-drop areas of Variable-stiffness Laminates on the strength. Their models consider the effect of in-plane ply waviness and the variable ply lay-ups at gaps and overlaps. In a similar way Fayazbakhsh. and Arian Nik et al [9,10] investigated the influence of in-plane ply waviness and variable stiffness induced by triangular gaps and overlaps at tow-drop areas on the buckling load. Both Lopes et al's and Fayazbakhsh et al's models ignored the out-of-plane waviness caused by gaps and overlaps. Most recently, Marrouze et al [11] developed the multi-scale progressive failure analysis (MS-PFA) approach to analyze the effect of isolated gaps on the strength and stability of composite structures. This MS-PFA method considers damage mechanics (strength, strain) formulation, load distribution and gradual degradation of mechanical properties at onset of damage. It used 2D unit cell models with cross-sections representative of the ply with a gap to produce stiffness and strength properties that are degraded due to the presence of gap defects. These properties are then applied to the structural level FE models with an identified distribution of gaps. Their work concluded that the reduction in compression strength caused by gaps is induced by the waviness in fibres. The degree of waviness is driven by the height of the gap, which depends on the tape thickness and not the gap length. Once the knockdown factor has peaked, increasing the gap length does not cause any further increase in knockdown factor. The MS-PFA method considers the fracture energy approach to consider the effect of defects in composites and builds a link between gap parameters and the ply waviness.

The above modeling work showed that the inhomogeneity and out-of-plane ply waviness as well as the sub-critical damage like splits and delamination need to be considered to accurately simulate the influence of gaps and overlaps. The inhomogeneity can be effectively modelled by considering the in-situ ply lay-up information at gaps and overlaps[3, 6-10], however there is a lack of effective way to include the out-of-plane waviness by various combination of gaps and overlaps. A ply-by-ply modeling technique with intra-ply

cohesive elements for splits and inter-ply cohesive elements for delamination has been developed in the University of Bristol [12] and successfully applied to modelling the open hole tension [13] and over-height compact tension tests [14] . In this paper 3D meshing tools were developed to automatically generate ply-by-ply gaps and overlaps models, in which both the out-of-plane waviness and the ply thickness variations are explicitly modeled. Cohesive elements for potential intra-ply splits and inter-ply delamination were inserted into the models. Models with various sizes and distribution of gaps and overlaps were built to predict the reduction of strength as a function of the magnitude and type of the defects. The results of the gap and overlap models will be used to guide future experimental characterization of simulated AFP process defects, manufactured by hand and laid up from pre-preg tape.

2. Features of gaps and overlaps in composites

To investigate the features of gaps and overlaps, trial specimens using IM7/8552 pre-preg with layup $[45/90/-45/0]_{2S}$ were made by hand and autoclave cured at the University of Bristol. Each of the plies is 0.25mm thick. 2mm gaps and overlaps were put in the innermost 45 plies. During the cure process two variants for the consolidation on the top surface of the specimens were used, one with soft tooling and one with hard tooling. The soft tooling used only release film, a layer of breather material and the vacuum bag. The hard tooling used a thick, flat aluminum plate in addition to the release film and breather material. The cure pressure under soft tooling condition is the same everywhere on the specimen, despite the local differences in overall laminate thickness.. Micrographic measurement of the cut-section images of specimens made with soft tooling shows that the ply thickness is nearly constant while the overall laminate thickness decreases at locations with gaps and increases at locations with overlaps. In contrast, the hard tooling changes the distribution of cure pressure, with higher pressure over overlaps and lower pressure over gaps. This causes local resin flow in the regions of gaps and overlaps. The micrographic images of specimens made with hard tooling show constant laminate thickness, despite the existence of internal gaps and overlaps. Examples of cut-section views of specimens made with soft tooling and hard tooling are shown in Fig. 3.

From the sectioned images in Fig 3, it was found that overlapping plies merged at the overlap zone and plies at gaps have a tendency to flow into and fill the gaps. In the case of gaps and overlaps being superimposed, the resin rich area and ply merging phenomena are enhanced.

Based on the above observations, simplified features for gaps and overlaps models were proposed as shown in Fig.4. For the gaps models, the ply has a length of A_{gap} to flow into the original gap. Away from the gap the ply within length B_{gap} was thinned down due to part of the ply material flowing into the gap. At the tip of the ply in the gap is a resin rich pocket with a length of R_{gap}. The thinnest part of the resin area has a minimum thickness of H_{min}. In overlap models, there is a transition area with length $A_{overlap}$ between the single ply and overlapped plies. A simplified interface was put between the two overlapped plies. The overlapped plies have a total increased thickness of $H_{overlap}$ as compared with a single ply. Both the ply thin down shape in the gap models and ply transition shape from single to overlapped plies follow cosine functions. For specimens manufactured by AFP with deposition pressure on the tapes or specimens with a different material system, the shapes of gaps and overlaps might be slightly different from the images in Fig. 3. In these cases, the three parameters: A_{gap}, B_{gap} and R_{gap} for defining the shape of gaps and two parameters: $A_{overlap}$ and $H_{overlap}$ for the shape of overlaps can be adjusted accordingly to get better defect shapes to fit to the real specimens.

For models with soft tooling, the ply thickness away from the regions influenced by gaps and overlaps is the same as in the pristine condition. Therefore the overall laminate thickness decreases at locations with gaps and increases at locations with overlaps. For models with hard tooling, the overall laminate thickness needs to remain constant, as for the pristine condition. Therefore the ply thickness over gaps needs to be increased and thickness over overlaps needs to be decreased. As the pressure on differently orientated plies in the thickness direction is similar during the cure process, the changes of fibre volume fraction due to the flow of resin were assumed to be the same for all plies regardless of orientation. Changes in ply thickness were averaged across the total laminate thickness. The in-situ fibre direction modulus $E_{11}(T)$ is a combination of the fibre modulus and the resin modulus based on their volume fracture. When the ply thickness changes the volume of fibre

remains constant and resin is squeezed out to accommodate the change. The in-situ ply modulus in the fibre direction $E_{11}(T)$ is thus modified as a function of the in-situ ply thickness:

$$E_{11}(T) = \frac{E_f V_{fo} T_o + E_{resin}[(1-V_{fo})T_o + (T-T_o)]}{T} = E_{11_0}\frac{T_o}{T} + E_{resin}\left(1 - \frac{T_o}{T}\right) \qquad (1)$$

where E_f is the fibre modulus, E_{resin} is the resin modulus, V_{fo} is the pristine fibre volume fraction, T is the in-situ ply thickness and To is the pristine ply thickness. $E_{11_0} = [E_f V_{fo} + E_{resin}[(1 - V_{fo})]$ is the pristine ply modulus.

The effect on shear, transverse and through-thickness moduli of the plies is sufficiently small that is can be considered to not be influenced by gaps and overlaps, i.e.

$E_{22}(T)=E_{22_0}$

$E_{33}(T)=E_{33_0}$

$G_{12}(T)=G_{12_0}$; $G_{13}(T)=G_{13_0}$; $G_{23}(T)=G_{23_0}$

Where (T) denotes the in-situ condition and the suffix "_0" denotes the pristine condition.

3. Meshes for gaps and overlaps models

In order to capture the splitting development in differently orientated plies, intra-ply cohesive elements were placed parallel to the fibre direction. To facilitate this, in-plane meshes for the gaps and overlaps models consist of unit cell meshes as shown in Fig. 5. The diagonal angle of the unit cell mesh can be adjusted to be applicable to differently oriented plies. For instance a quasi-isotropic layup consisting of 0°, 90° and ±45° plies uses the unit cell mesh as shown in Fig. 5a. For a layup consisting of 0°, 90° and ±30° plies, the unit cell mesh is shown as Fig. 5b.

By inputting the unit mesh size, the dimension of each ply and the spacing of pre-defined splits in the plies, the meshing tools can generate the basic mesh for each oriented ply. Cohesive elements for intra-ply splits are put at interfaces between different areas.

The distribution of gaps and overlaps within a ply can be expressed by an array [no. of ply, x_c, y_c, gap or overlap size], where 'no. of ply' identifies the ply in which to put gaps and overlaps, (x_c, y_c) are the in-plane coordinates of the centre, and 'Gap or overlap size' defines the width. Positive value of the size represents an overlap and negative size means a gap.

By inputting the stacking sequence and distribution of gaps and overlaps, the meshing tool generates the meshes with defects. Cohesive elements are generated between all plies to capture potential delaminations. For the model with the hard tooling condition, the ply thickness is automatically adjusted based on the assumption in section 2 to get constant laminate thickness at regions with gaps and overlaps. For the soft tooling model the plies were assumed to have no thickness change due to the flexible upper surface. Fig. 6 gives an example of such a mesh with layup $[45/90/-45/0]_{3s}$ and gap distribution array as:

[3, x_o, y_o, 2]

[7, x_o+10, y_o+10, 2]

[11, x_o+20, y_o+20, 2]

[14, x_o, y_o, 2]

[18, x_o+10, y_o+10, 2]

[22, x_o+20, y_o+20, 2]

The overlap distribution array is:

[3, x_o, y_o, -2]

[7, x_o+10, y_o+10, -2]

[11, x_o+20, y_o+20, -2]

[14, x_o, y_o, -2]

[18, x_o+10, y_o+10, -2]

[22, x_o+20, y_o+20, -2]

The finite element meshes if the individual plies with gaps and overlaps, as shown in Fig.6. were then stacked up with the meshing tool to form a laminate model as shown in Fig. 7, with cohesive elements generated

between plies to capture the potential delaminations. Cut-section views of the model in Fig. 7a. show the existence of gaps and overlaps in the model. Fig. 7b. gives close 3D views of the gaps and overlaps. For trial specimens with the layup $[45/90/-45/0]_{2S}$, the generated models have very similar cut-section views to the specimens, as shown in the Fig. 8.

All models have an in-plane dimension of 30mmx70mm. The thickness is 4mm for 16 plies and 6mm for 6mm for 24 plies. To accurately capture the features of defects, the in-plane mesh size should be no larger than any of the defect parameters: A_{gap}, B_{gap}, R_{gap} for gaps models and $A_{overlap}$ for overlaps models. Measured parameters from the trial specimens are: $A_{gap}=0.42mm$, $B_{gap}=0.50mm$, $R_{gap}=0.56mm$ and $A_{overlap}=0.78mm$. A thermal load with temperature decreasing from 180 °C to 20 °C was applied to each model before mechanical loading to account for residual stresses due to cool down from the cure temperature. During the mechanical loading using a prescribed displacement the two ends were constrained in the thickness direction to simulate the gripping by the loading fixture . Constant stress solid elements were used (one integration point) . Local orthotropic material axes were determined, as shown in Fig. 9, by rotating the material axes ***a*** about the element normal ***N*** by an angle, β, from a vector *X* on the mid-surface of the element, defined by the cross product of the vector ***V*** with the element normal ***N***. Beta is the angle of ply orientation, e.g. for a 45° ply Beta is 45°. The vector *V* is a user defined vector on the mid-surface of the element and transverse to the ply waviness. The vector ***X*** lies on the mid-surface of the element and parallel to the ply waviness. The mid-surface of the element is between the inner surface and outer surface defined by the first four nodes and the last four nodes of the connectivity of the element, respectively.

Initial work compared model results using mesh sizes of 0.2mm and 0.35mm. The 24 ply models have 2.1 million elements using the 0.2mm mesh size and 1.2 million elements using the 0.35mm mesh size. Models were run in the explicit finite element code LS-Dyna on the University of Bristol BlueCrystal High Performance Computer using two Xeon E5-2670 2.6GHz 8 core processors with 64 GB RAM. Total CPU times for the models with 2.1million and 1.2 million elements are 16 hours and 9 hours respectively. Both models gave similar results. The comparison showed that this modelling approach using cohesive elements

and the Weibull statistical fibre failure criterion has a good convergence and mesh independence when the mesh sizes are smaller than the defect parameters. In models presented in the rest of this paper, a mesh size of 0.35mm was used.

4. Failure Criteria

Cohesive elements inserted in gaps and overlaps models for intra-ply splitting and inter-ply delamination used a bi-linear traction-displacement curve with a strength based initiation and fracture energy based propagation criterion [7]:

$$\left(\frac{<\sigma_1>}{\sigma_I^{\max}}\right)^2 + \left(\frac{\sigma_{II}}{\sigma_{II}^{\max}}\right)^2 = 1 \qquad (2)$$

$$<\sigma_1> = \begin{cases} \sigma_1 & \sigma_1 > 0 \\ 0 & \sigma_1 \le 0 \end{cases}$$

$$\left(\frac{G_I}{G_{IC}}\right) + \left(\frac{G_{II}}{G_{IIC}}\right) = 1 \qquad (3)$$

Where σ_1 and σ_{II} are mode I and mode II stresses, $\sigma_I^{\max}$ and $\sigma_{II}^{\max}$ are mode I and mode II maximum stresses. G_I and G_{II} are mode I and mode II fracture energies, G_{IC} and G_{IIC} are critical energy release rates for mode I and mode II respectively.

The Weibull statistical failure criterion in Equation (4) [15] integrates the stresses over the entire model to account for the strength variability and size effect on tensile strength based on equal probability of failure. Equation (4) is implemented within the ply solid elements to capture the fibre tensile failure.

$$\sum_{i=1}^{No.\,Solid\,Elements} V_i \left(\frac{\sigma_i}{\sigma_{unit}}\right)^m = 1 \qquad (4)$$

Where σ_{unit} is the unidirectional failure strength of unit volume of material and m is the Weibull modulus. σ_i and V_i are the elemental longitudinal tensile stress and volume respectively. When the fibre failure criterion in Equation (4) is satisfied, the element with the maximum fibre direction stress loses its load carrying capability and is removed from the model. The load is automatically redistributed to other remaining elements by the FEA program. With the loading continuing, stresses keep increasing until Equation (4) is satisfied again, then a further element with the maximum longitudinal tensile stress in the model at this time step is removed. In this way, the progressive fibre failure in the gaps and overlaps specimens is simulated. Further details of this model can be found in [15]. When the ply thickness changes due to the gaps and overlaps, it is assumed that its failure probability is the same as in the pristine condition at the same strain level and that the Weibull modulus *m is* not influenced by the variations of V_f,. The in-situ Weibull unit strength $\sigma(T)_{unit}$ is determined by:

$$V_i(T)\left(\frac{E_{11}(T)\varepsilon_{11}}{\sigma(T)_{unit}}\right)^m = V_{i_0}\left(\frac{E_{11_0}\varepsilon_{11}}{\sigma_{unit\ 0}}\right)^m \qquad (5)$$

Where (T) denotes the in-situ condition and the suffix "_0" denotes the pristine condition.

. As $\frac{V_i(T)}{V_{i_0}} \approx \frac{T}{T_0}$, we get:

$$\sigma(T)_{unit} = \left(\frac{T}{T_0}\right)^{1/m}\frac{E_{11}(T)}{E_{11\ 0}}\sigma_{unit_0} \qquad (6)$$

By combining Equation (1) and Equation (6), $\sigma(T)_{unit}$ is obtained as a function of the in-situ ply thickness T:

$$\sigma(T)_{unit} = \left(\frac{T}{T_0}\right)^{1/m}\left(\frac{T_0}{T} + \frac{E_{resin}}{E_{11_0}}\left(1 - \frac{T_0}{T}\right)\right)\sigma_{unit_0} \qquad (7)$$

For compressive failure, the simple maximum stress failure criterion as in Eqation(8) was used.

$$\sigma_{11} > X_c \qquad (8)$$

Where σ_{11} is the fibre direction stress, X_c is the compressive strength. When the fibre direction stress exceeds the compressive strength, the specimen is taken to experience a sudden and catastrophic failure.

Fig. 10 gives the flow chart for the simulation process.

5. Comparison of models for hard tooling and soft tooling condition

To compare the difference between models built using hard tooling and soft tooling assumptions, the layup and defect distribution as shown in Fig. 11. was used. Each of the plies is 0.25mm thick and the total laminate thickness is 4mm. The material was Hexcel's IM7/8552 pre-preg with the properties listed in Table 1 for plies and Table 2 for cohesive elements. The cohesive element fracture properties used are a best fit to experimental mixed mode fracture data from [16]. For the cohesive element maximum stresses, typical values for epoxy matrix material were used, which have been shown to give successful simulations in previous analyses [12, 13, 14]. Since it is the propagation of the matrix cracks and delaminations that are the significant events, rather than their initiation, the exact value used for these latter parameters is less critical than the fracture data. In the configuration of Fig. 11, 2mm wide gaps and overlaps were generated simultaneously by shifting a strip of 6mm wide tape. Cut section views of the models, taken along the length of the specimen and at the centre across the width, for hard tooling and soft tooling are compared in Fig. 11b and c. To enhance the visibility, the ratio in the thickness direction of the section was increased by a factor of 1.5 so that the ply waviness inside the laminate looks more severe than the actual case. It can be seen that the model for hard tooling has a flat top surface and the model for soft tooling has an undulating surface. The ply waviness in the hard tooling model is less than that in the soft tooling model.

Both hard tooling and soft tooling models failed by delamination before fibre failure criteria was satisfied. The delamination initiation location can be identified both in-plane and in the through-thickness direction in the model, as shown in Fig. 12. After initiation, the delamination propagated across the whole width of the model and caused the complete failure. Gross section stress vs. tensile strain curves of the two models are compared in Fig.13. in which the hard tooling model has an obviously larger failure initiation stress and final failure stress. Delamination at the point of initiation and also the start of the load drops is visually shown in Figure 13. In both soft tooling and hard tooling models delamination initiated at the centre of the specimen and then gradually propagated across the width towards both edges. In the soft tooling model the delamination

propagated more quickly to one edge than the other. In the hard tooling model the delamination propagated symmetrically to both edges. Initially the delamination is highly localised and so does not greatly affect the load carrying capability. In both models the load curves therefore did not drop until the delamination had become more extensive and reached the specimen edges. This comparison suggests that hard tooling can help reduce the ply waviness at gaps and overlaps and thus increase the tolerance to such defects in terms of strength at failure initiation, the maximum strength and the post damage behaviour. All other models studied in this paper have similar shape of stress/strain curves and failure modes, only the failure loads are different. To avoid too many figures in the paper, only failure loads of other models were compared.

6. Batch analysis of gaps and overlaps models

To test the reliability of the meshing tool, pristine IM7/8552 models with no defects and layup $[45/90/-45/0]_{3S}$ were firstly created and simulated in both tension and compression. The pristine models failed by delamination (initiating from the edges then propagating across the width) before fibre failure in tension and by fibre failure before any delamination happened in compression. The model failure modes in both tension and compression well match the experimental results obtained through in house testing at the University of Bristol. Table 3 gives the comparison of test results[17] for the pristine specimen with the results predicted by the models. The good agreement between tests and models for the pristine layup in both the tension and compression cases suggests that the distribution of cohesive elements for splitting and delamination and the failure criteria for the cohesive and solid elements are reasonable.

A series of defect models with layup $[45/90/-45/0]_{3S}$ were then created using the meshing tools and simulated in both tension and compression. The defects are across the whole width of the specimen with the defect size varying between 0 and 4mm, the percentage area of the defects varying between 0 and 5.7%. 4mm is the maximum defect size that was considered possible to occur in production by the project industrial partner. The influence of orientation of isolated defects was firstly investigated. In the defect models, either gaps or overlaps were placed only in the 90° plies (as shown in Fig. 14a.), and only in the 45° or -45° plies (as shown

in Fig. 14.b) with or without stagger. The defect size was 2mm and figure 14 shows a schematic cut section in the loading direction, with the relative location of the defect seeds highlighted. For defect seeds without stagger the defects were aligned in the through-thickness direction. For defect seeds with stagger, the stagger distance is 10mm to create through-thickness ply waviness between defects. The material propertyies values used are shown in Table 1 for the plies and Table 2 for the cohesive elements. The normalized tensile and compressive strength of the defect models were compared with pristine models in Fig. 15, in which labels of the models are in the format of; orientation of defects (90° ply, -45° ply or $+45^o$ ply)+defect types (gap or overlap)_stagger type (stagger1 or stagger2). The modeling demonstrated that gaps and overlaps cause larger strength knock-down in compression than in tension. Defects in the 45° or -45° plies have a larger effect on the failure than defects in the 90° plies. Defects in 45° and -45° plies have a similar effect on the failure. In 45° and -45° plies, gaps have larger knock-down than overlaps in both tension and compression. On the contrary, in 90 plies overlaps caused much larger knock-down than gaps in both tension and compression, which is quite counter intuitive and need further validation in future work. Defects with the stagger 1 have larger strength knock-down than those with stagger 2. This can be explained by the fact that stagger 1 aligned the defects in the thickness direction and thus enhanced the out-of-plane ply waviness.

To investigate the influence of defect size, stagger distance and stagger repeat, another series of gaps and overlaps models with layup $[45/90/-45/0]_{3S}$ and defects only in the -45° plies were created using the meshing tools. This series of models include gaps or overlaps only in the -45° plies with a positive stagger distance as shown in Fig. 16a, negative stagger distance as shown in Fig. 16b and combination of gaps and overlaps in -45° plies with negative stagger distance as shown in Fig. 16c. All cases were studied with defects only in the -45° plies. The normalized tensile and compressive strength for models with different defect sizes and the same positive stagger distance of 10mm are shown as curves in Fig. 17. The effect of stagger distance with a 4mm defect size on the tensile strength and compressive strength is presented in Fig.18 and Fig. 19 respectively. It was further found that negative stagger distance has the largest influence on the failure of the defect models. Although curves in Fig. 16 show increased strength knock-downs with the increased defect sizes, the

overall knockdowns by the different defect sizes are still very small absolute values. Therefore, the influence of varying the defect size is considered as minor. It can also be found from Fig. 18 and Fig. 19 that stagger repeat and positive stagger distance have a minor influence on the failure. For isolated defects without interacting, the out-of-plane ply waviness is mainly influenced by the thickness of ply and parameters of the defect features: A_{gap}, B_{gap}, R_{gap} for gaps and $A_{overlap}$, $H_{overlap}$ for overlaps. There are thresholds for defect size, below which the defect size influences the out-of-plane ply waviness and above which the out-of-plane ply waviness is independent of the defect size. The threshold value for isolated gaps would be $2(A_{gap}+R_{gap})$. For overlaps, the threshold is $2A_{overlap}$. For interacting defects with stagger, the defects with larger size than the threshold may interact with the stagger distance. In such cases, the defect size above the threshold also has influence on the out-of-plane waviness. For the tension cases with negative stagger distance and the same defect size, the influence of overlaps is greater than gaps, with gaps+overlaps in combination having the least effect. For cases of compression with negative stagger distance and the same defect size, the influence of Gaps is greater than Gaps+Overlaps in combination with Overlaps having the least effect. Reasons for these trends might be that the ply waviness caused by gaps is larger than that caused by overlaps. The ply waviness caused by overlaps is well supported by the intensely squeezed adjacent plies, but the ply waviness caused by gaps is less well supported due to the resin rich areas which develop at gaps. In general, the knockdown due to gaps will be smaller in tension than compression due to the effect waviness causes being less severe. It is mainly the transition areas, not the whole length of the gaps and overlaps that influence the ply waviness. This can explain the decrease-increase-decrease trend of the strength when the stagger distance reduced from 0mm to -4mm in Fig. 20, since at stagger distance 0mm and -4mm the transition areas of the defects were aligned while at stagger distance -2mm the transition areas of defects were misaligned, causing greater waviness. Fig. 17 and Fig. 18 also show that the stagger distance has less impact on the strength for the case of gaps compared to overlaps. This can be explained by the fact that the flow of resin into gaps and the bridging effect by surrounding fibres on the plies over the gap help to smooth the out-of-plane ply waviness. In this way the staggering effect of gaps on the ply waviness was greatly reduced during the curing process. For specimens with overlaps, the ply waviness follows the adjacent plies more closely with no resin pockets developing, therefore overlaps are more sensitive to the stagger pattern. The features of gaps and overlaps models in

this paper consider the effect of resin flowing into gaps and the ply thickness change at gaps and overlaps, therefore they can reflect the different impact of the stagger distance on gaps and overlaps.

7. Discussion and future work

A sophisticated meshing tool has been developed to automatically create complex models of gaps and overlaps specimens. This meshing tool makes it easy to create series of defect models with various combinations and permutations of gaps and overlaps, hence to systematically investigate the influence of defect size and distribution on the strength knockdown of the specimens. Cross-section views of gaps and overlaps in the models generated automatically from a set of predefined parameters showed very good agreement with views of manufactured specimens. Both tensile strength and compressive strength of pristine models generated by the meshing tool have a good agreement with the test results, showing good potential for the meshing tool for gaps and overlaps models. Results from batch analysis of the defect models with both isolated gaps and overlaps and interacting gaps and overlaps are encouraging, though they still need to be verified against tests in the future.

The isolated defects investigated thus far may not represent the worst strength knockdown due to gaps and overlaps. To further investigate the effect of defects interacting with each other, more complex models can be built, such as those shown in Fig. 20 and Fig. 21. In Fig. 20 defect seeds are put in the innermost 45, 90 and -45 plies. At the in-plane cross-over point these defects give rise to a “stack up” of the gaps or overlaps as shown in Fig. 20a. For the stacked up gaps and overlaps models, the cross-over centre of the defects can be close to either edge or at the centre of specimen, as shown in Fig.20b. Cut-section views of the superimposed gaps and overlaps at cross-over point are shown in Fig. 20c and d. In Fig. 21a, additional defect seeds are put in the external 45, 90 and -45 plies with a stagger from the inner most defects seeds as in Fig. 20a. Defect seeds in Fig. 21b consider the combination of gaps and overlaps. Fig. 21c shows a possible coupling of gaps and overlaps with various defect sizes. To apply these more complex models, further experimental validation is required, first for the isolated defect models and then also the geometric effects of the interacting defects.

With detailed finite element analysis such as this it will become possible to generate guidelines for the tolerance of specimens made by AFP to gaps and overlaps.

Acknowledgements

The authors would like to acknowledge the support of Rolls-Royce plc for their support of this research through the Composites University Technology Centre (UTC) at the University of Bristol, UK.

References

[1] Debout P , Chanal H , Duc E. "*Tool path smoothing of a redundant machine: Application to Automated Fiber Placement".* Computer-Aided Design. Vol 43, no 2, pp122-132, 2011.

[2] Sawicki AJ, and Minguet PJ. "*The Effect of Intraply Overlaps and Gaps Upon the Compression Strength of Composite Laminates*", AIAA/ASME/ASCE/SHS/ASC Structures, Structural Dynamics &Materials Conference, Vol. 1, pp744-754, . 1998.

[3] Turoski, LE. "*Effects of Manufacturing Defects on the Strength of Toughened Carbon/Epoxy Prepreg Composites*", MSc Thesis, Montana State University, 2000.

[4] Croft K, Lessard L, Pasini D, Hojjati M and Chen JH and Yousefpour A. "*Experimental study of the effect of automated fiber placement induced defectson performance of composite laminates*", Composites: Part A, Vol. 42, pp 484–491, 2011

[5] Cairns DS, Ilcewicz LB, and Walker T. "*Far-Field and Near-Field Strain Response of Automated Tow-Placed Laminates to Stress Concentrations*", Composites Engineering, Vol. 11, no.3, pp1087-1097, 1993

[6] Lopes CS, Gürdal Z, Camanho PP. "Variable‐stiffness composite panels: buckling and first‐ply failure improvements over straight‐fibre laminates". Computers & Structures. Vol. 86, pp897‐907, 2008

[7] Lopes CS, Camanho PP, Gürdal Z, Tatting BF. "Progressive failure analysis of tow‐placed, variable‐stiffness composite panels". International Journal of Solids and Structures. Vol. 44, pp8493‐516, 2007

[8] Blom AW, Lopes CS, Kromwijk PJ, Gürdal Z, Camanho PP. "A theoretical model to study the influence of tow‐drop areas on the stiffness and strength of variable‐stiffness laminates". Journal of Composite Materials. Vol. 43, pp403‐25, 2009.

[9] Fayazbakhsh K, Arian Nik M, Pasini D and Lessard L. "Defect Layer Method to Capture Effect of Gaps and Overlaps in Variable Stiffness Laminates made by Automated Fiber Placement", Composite Structures Vol. 97, pp. 245–251, 2013

[10] Arian Nik M, Fayazbakhsh K, Pasini D and Lessard L. "Optimization of variable stiffness composites with embedded defects induced by Automated Fiber Placement", Composite Structures, Vol. 107, pp. 160–166, 2014.

[11] Marrouze JP, Housner J, and Abdi F." Effect of manufacturing defects and their uncertainties on strength & stability of stiffened panels", ICCM19, Montreal Canada, July 2013.

[12] Jiang WG, Hallett SR, Green BG, Wisnom MR. "A concise interface constitutive law for analysis of delamination and splitting in composite materials and its application to scaled notched tensile specimens". Int J Numer Methods Eng, Vol 69, pp1982–95, 2007.

[13] Hallett SR, Green BG, Jiang WG, Cheung KH and Wisnom MR. "The Open Hole Tensile Test - A Challenge For Virtual Testing of Composites", International Journal of Fracture, Vol 158(2), pp169-181, 2009

[14] Hallett SR, Green BG, Jiang WG, Wisnom MR. "An experimental and numerical investigation into the damage mechanisms in notched composites",Composites Part A, Vol 40, pp613-624, 2009

[15] Li X, Hallett SR, Wisnom MR. "A finite element based statistical model for progressive tensile fibre failure in composite laminates". Composites Part B: Engineering. Vol 45, no 1, pp433–439, 2013.

[16] Jimenez MA, Miravete A. " Application of the finite-element method to predict the onset of delamination growth". Journal of Composite Materials. Vol 38, no15, pp1309-1335, 2004.

[17] Jones MI. "Defect and features test report", University of Bristol, 2013.

Published in Science and Engineering of Composite Materials 2015; 22(2): 115–129
DOI 10.1515/secm-2013-0322

Figures

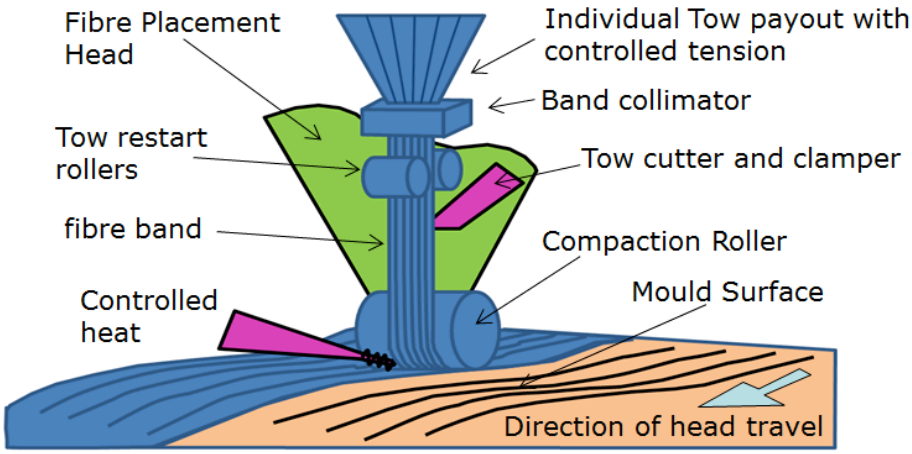

Fig. 1. Automated Fibre Placement head[1]

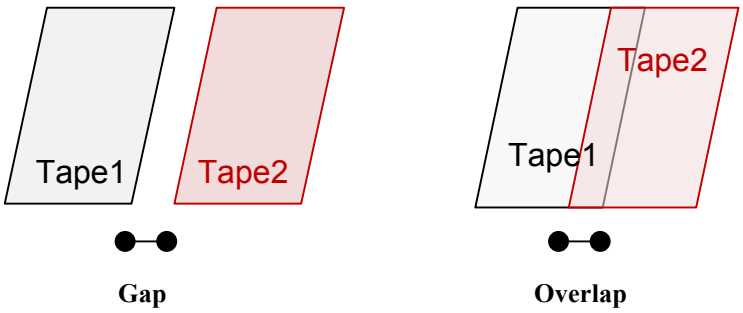

Fig. 2. Schematic gap and overlap between adjoining tapes

Published in Science and Engineering of Composite Materials 2015; 22(2): 115–129
DOI 10.1515/secm-2013-0322

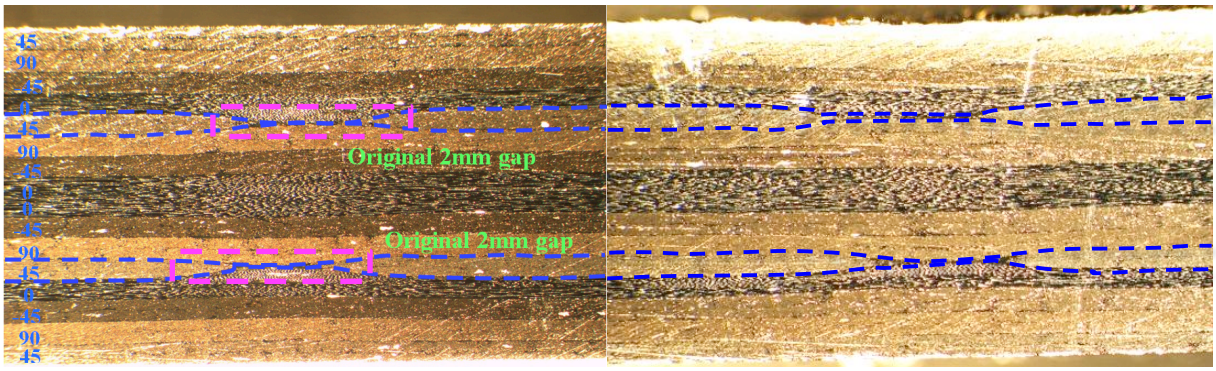

a. Gap with hard tooling b.Gap with soft tooling

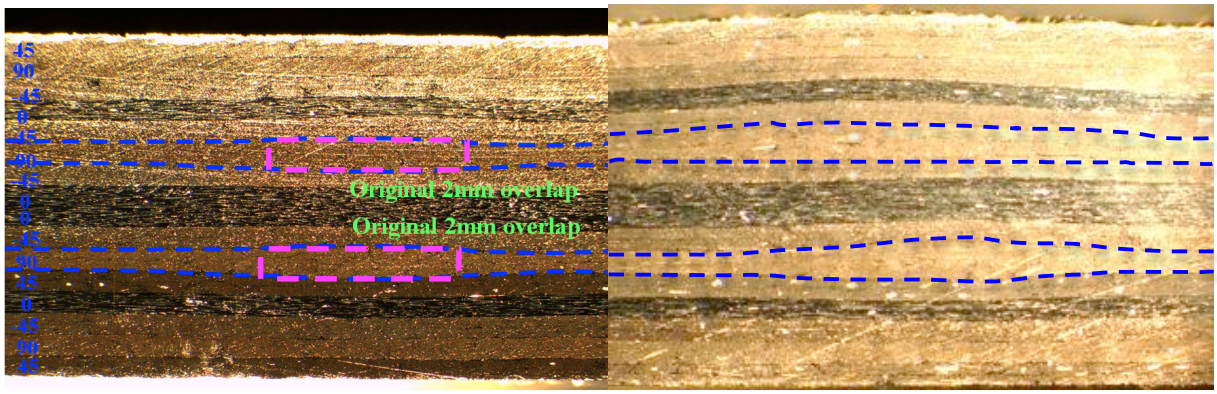

b. Overlap with hard tooling d. Overlap with soft tooling

Fig. 3. Cut-section view of gaps and overlaps trial specimens with soft and hard tooling

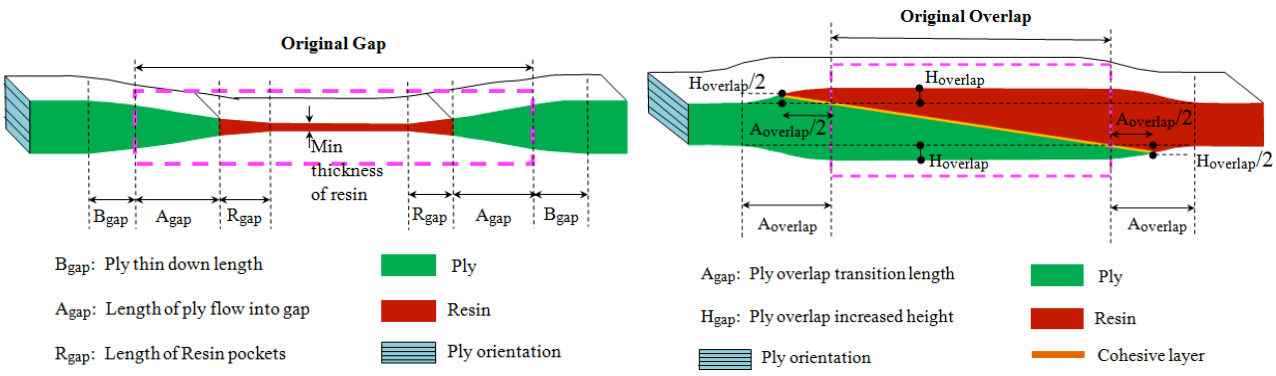

Feature for Gaps models Feature for Overlaps models

Fig. 4. Simplified features of gaps and overlap models

Published in Science and Engineering of Composite Materials 2015; 22(2): 115–129
DOI 10.1515/secm-2013-0322

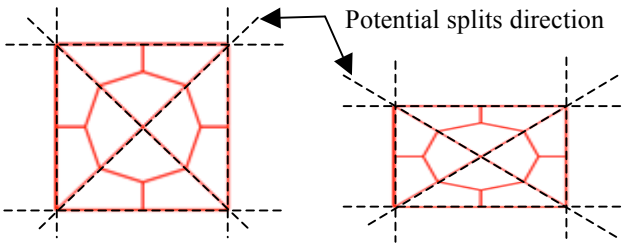

a. for 45°, -45°ply b. for 30°,-30°ply

Fig. 5. Unit cell for the meshes of gaps and overlaps models

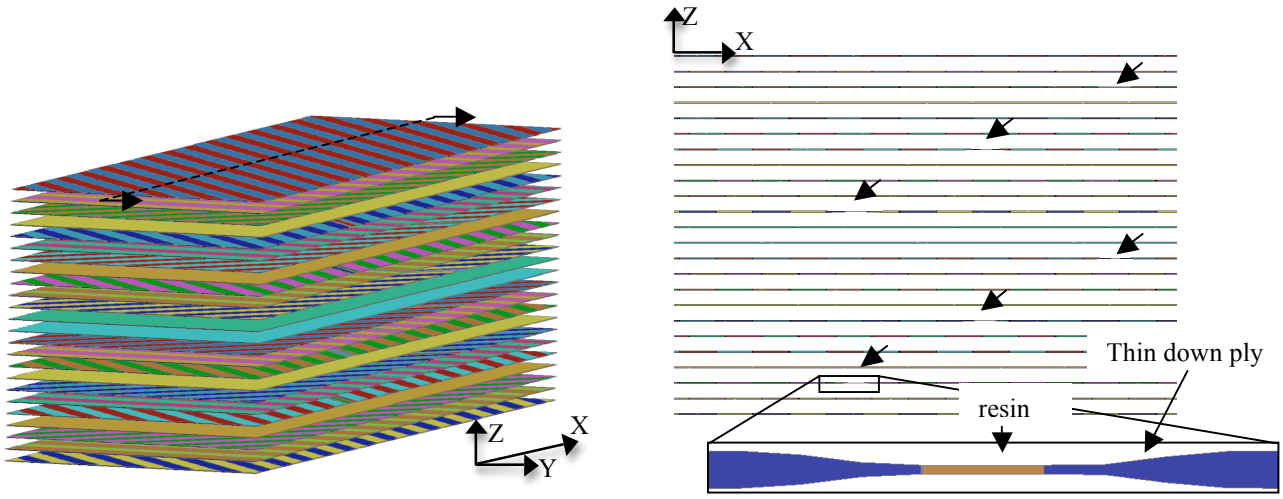

a.mesh with layup[45/90/-45/0]$_{3s}$ b. cut-section views of distributed gaps

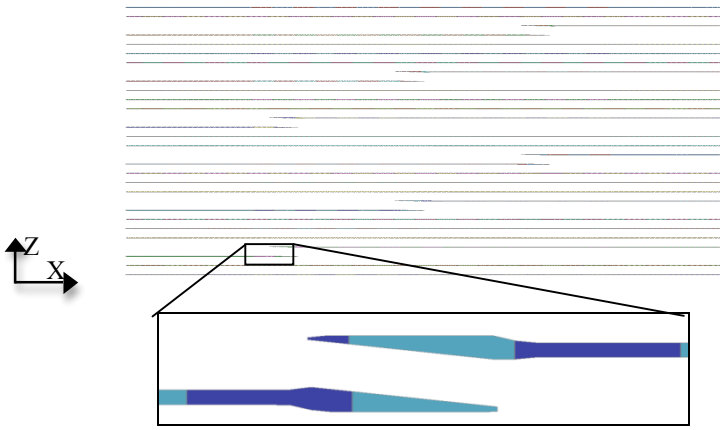

c. cut-section views of distributed overlaps

Fig.6. Mesh with layup [45/90/-45/0]$_{3s}$ and cut-section views of distributed gaps and overlaps

Published in Science and Engineering of Composite Materials 2015; 22(2): 115–129
DOI 10.1515/secm-2013-0322

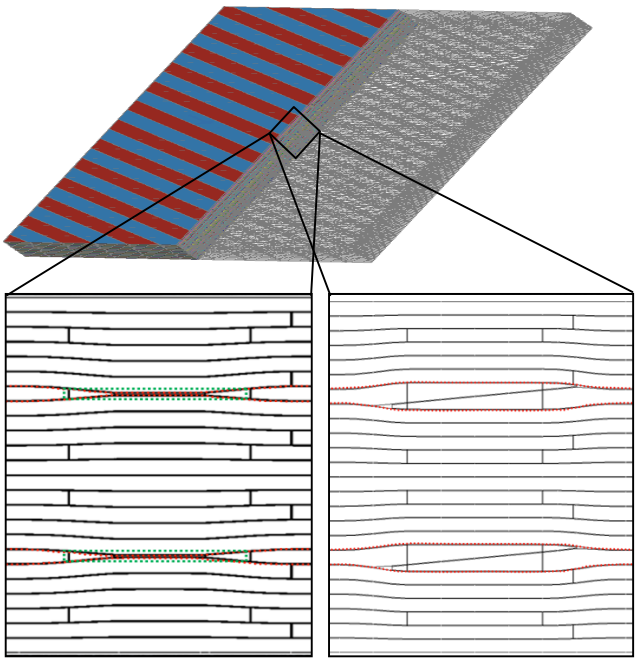

gaps overlaps

a. cut-section views of gaps and overlaps in the model

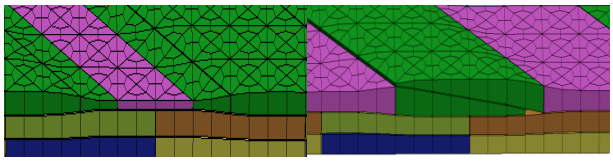

Gap overlap

b. 3D views of gaps and overlaps in the model

Fig.7. Gaps and overlaps model with a stacking sequence $[45/90/-45/0]_{3S}$

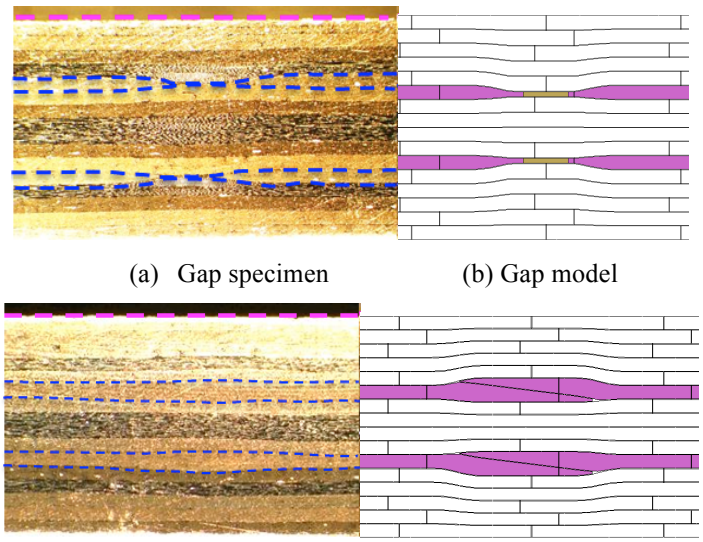

(a) Gap specimen (b) Gap model

(c) Overlap specimen (d) Overlap model

Fig.8. Cross-section views of isolated gaps and overlaps in the specimens and the models

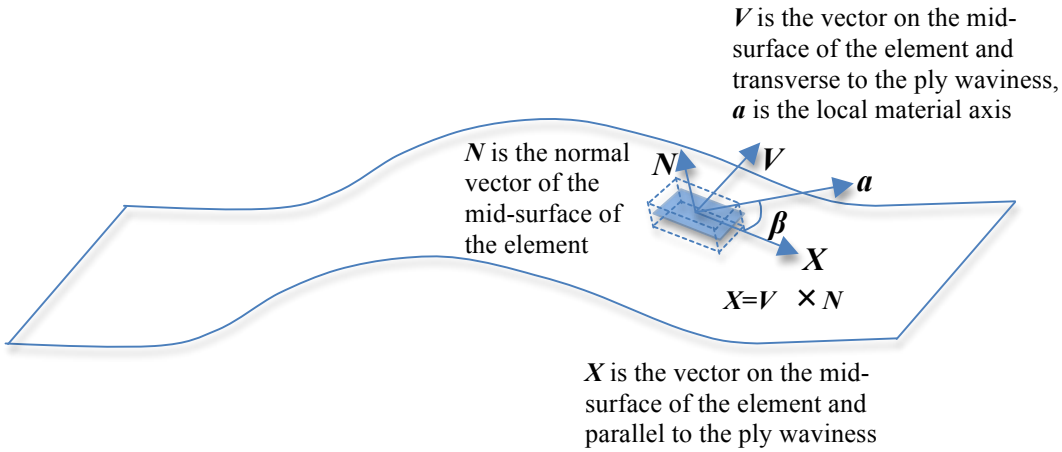

Fig.9. Determination of the local material axis *a* in an element at the ply waviness

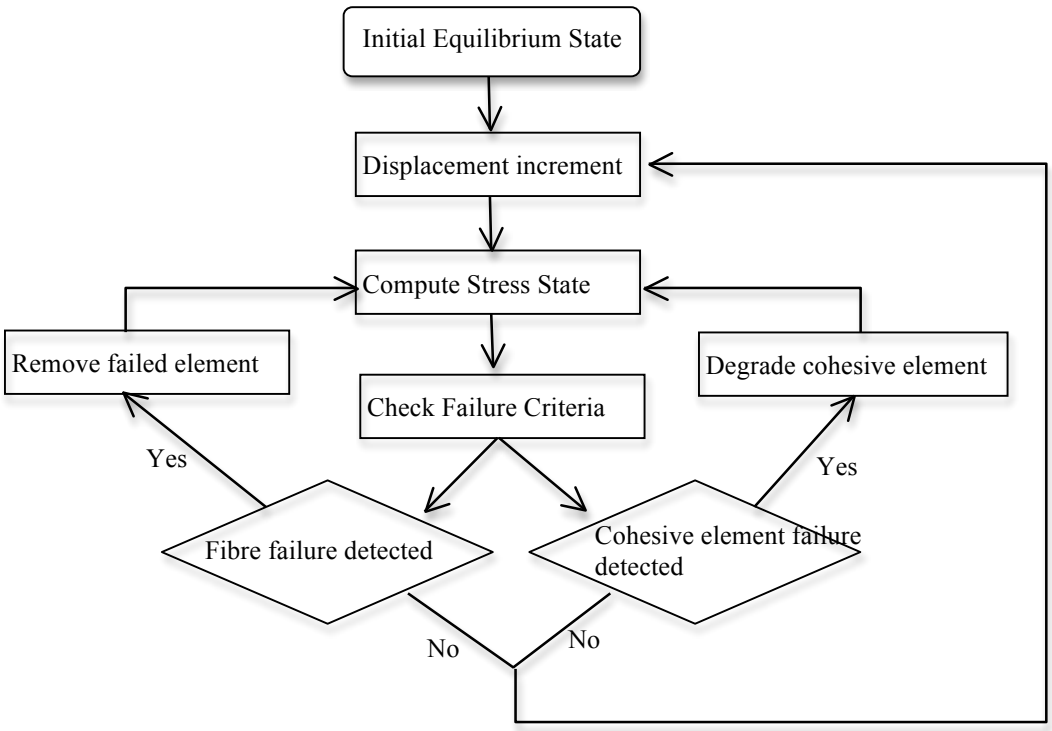

Fig.10. Flow chart for the FE analysis of the defect models

Published in Science and Engineering of Composite Materials 2015; 22(2): 115–129
DOI 10.1515/secm-2013-0322

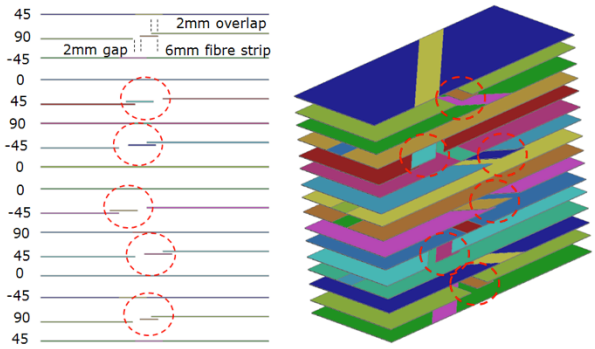

a. defects distribution

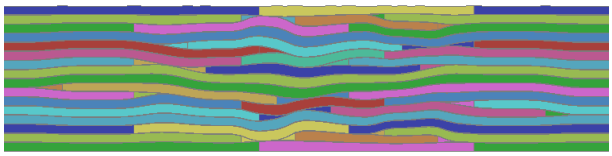

b. cut-section view of the model for hard tooling

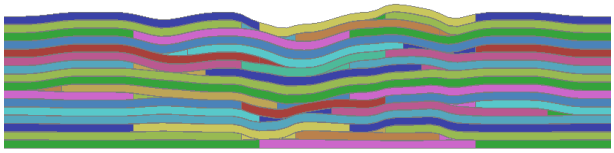

c. cut-section views of the model for soft tooling

Fig. 11. Comparison of cut-section views of models for hard and soft tooling, thickness changes magnified

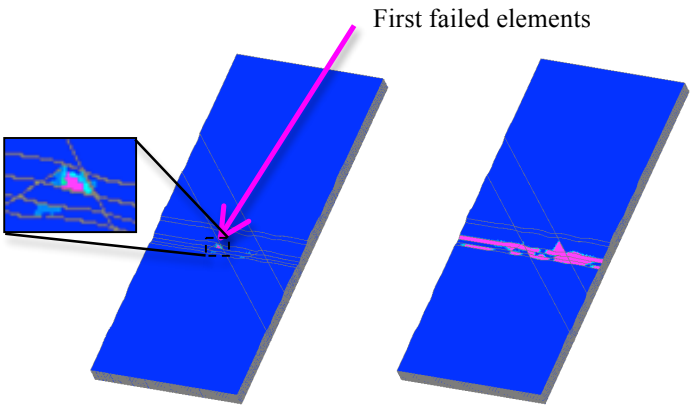

Delamination initiation delamination propagation

Fig. 12. Failure (delamination) intiation and propagation within the hard tooling model

Published in Science and Engineering of Composite Materials 2015; 22(2): 115–129
DOI 10.1515/secm-2013-0322

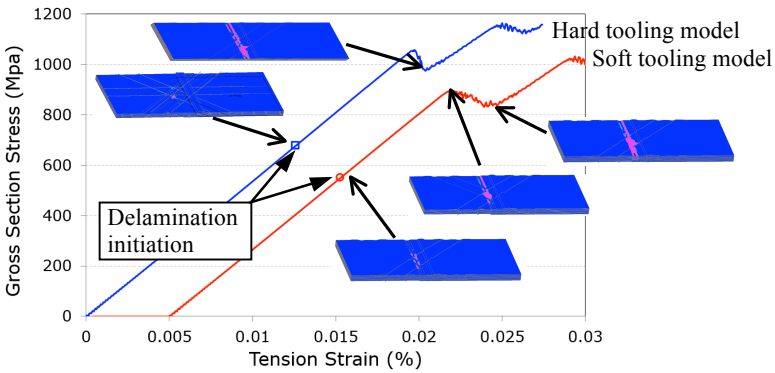

Fig.13. Comparison of failure stresses of hard tooling and soft tooling models

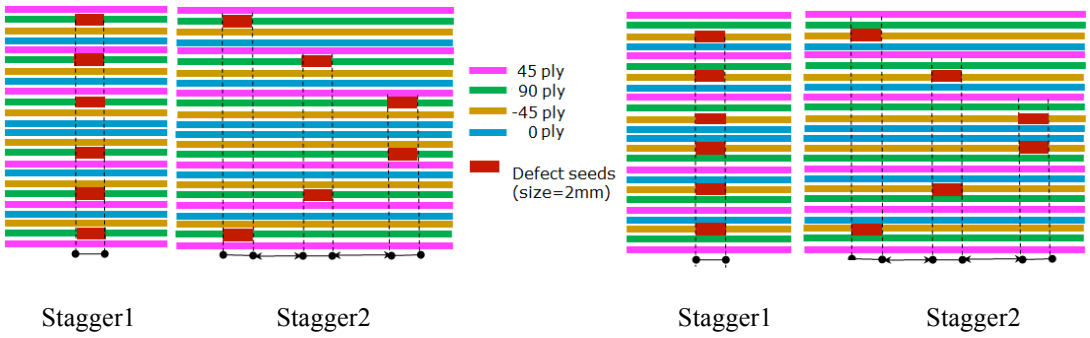

a. Gaps or overlaps only in 90° plies

b. Gaps or overlaps only in -45° plies

Fig. 14. Gaps and overlaps only in 90° and -45° plies with or without stagger

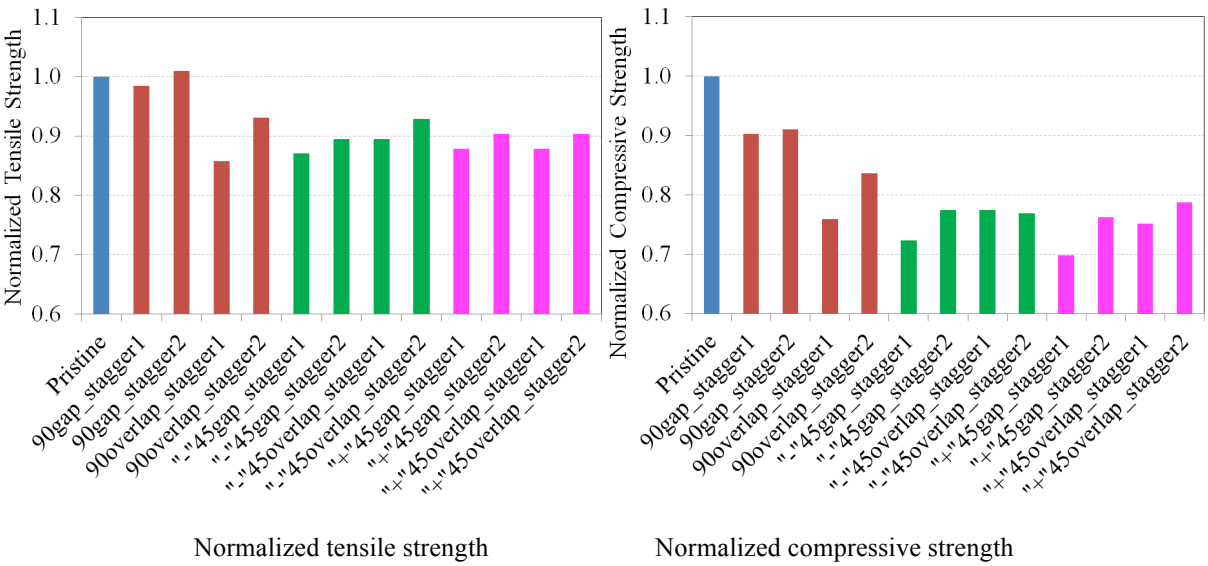

Fig 15. Normalized strength of gaps & overlaps models vs. defect orientations

Published in Science and Engineering of Composite Materials 2015; 22(2): 115–129
DOI 10.1515/secm-2013-0322

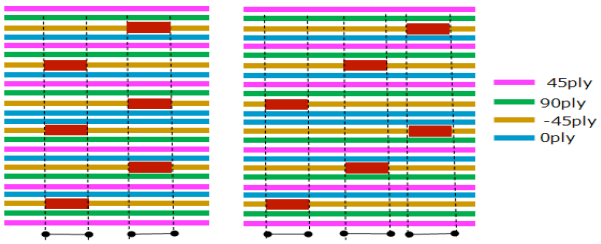

Stagger 1 Stagger2
a.only gaps or overlaps with positive stagger distance

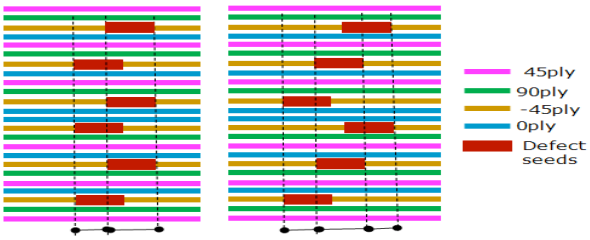

Stagger 1 Stagger2
b.only gaps or overlaps with negative stagger distance

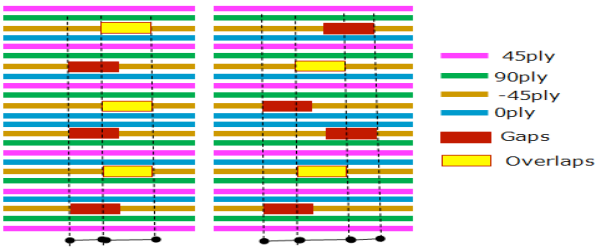

Stagger 1 Stagger2
c. combination of gaps and overlaps with negative stagger distance

Fig.16. Different models run with defects in -45°plies only

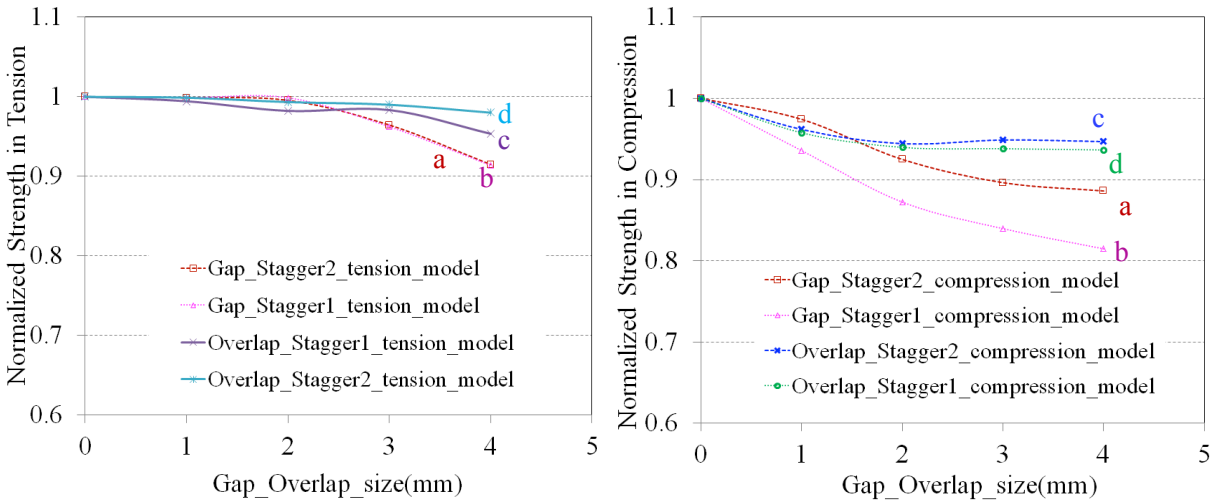

Fig.17. Normalized tensile strength and compressive strength vs. defect size for 45° defects models with a positive stagger distance of 10mm

Published in Science and Engineering of Composite Materials 2015; 22(2): 115–129
DOI 10.1515/secm-2013-0322

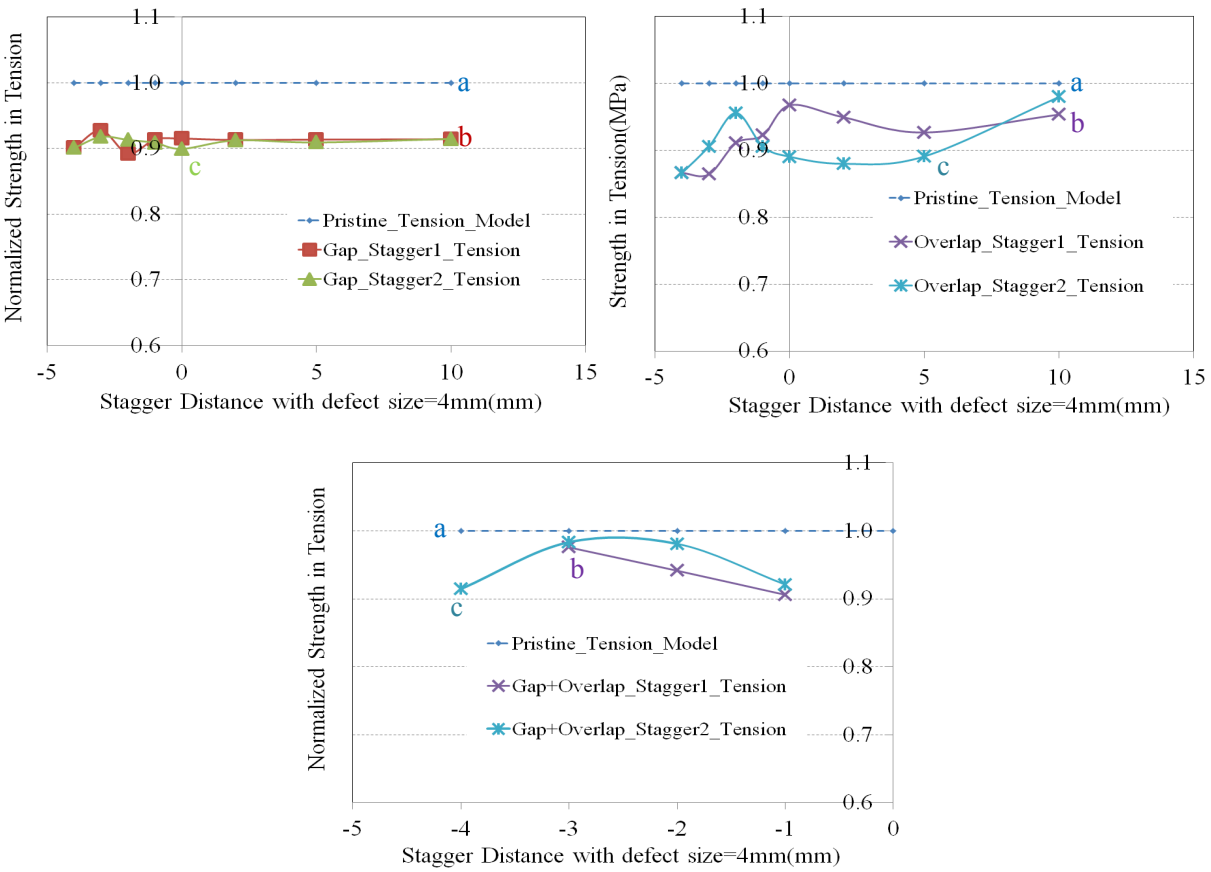

Fig.18. Normalized tensile strength vs. stagger distance with 45° defect size=4mm

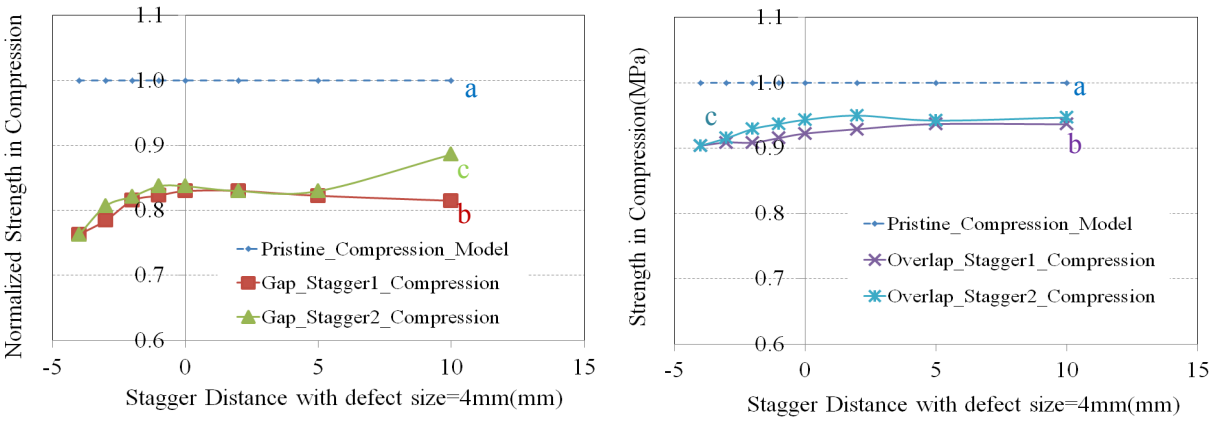

Published in Science and Engineering of Composite Materials 2015; 22(2): 115–129
DOI 10.1515/secm-2013-0322

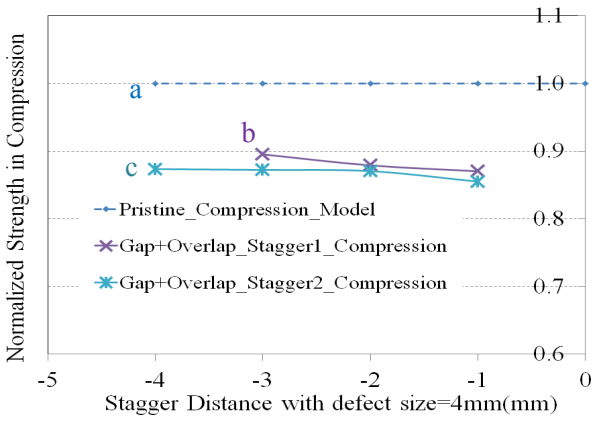

Fig.19. Normalized compressive strength vs. stagger distance with 45° defect size=4mm

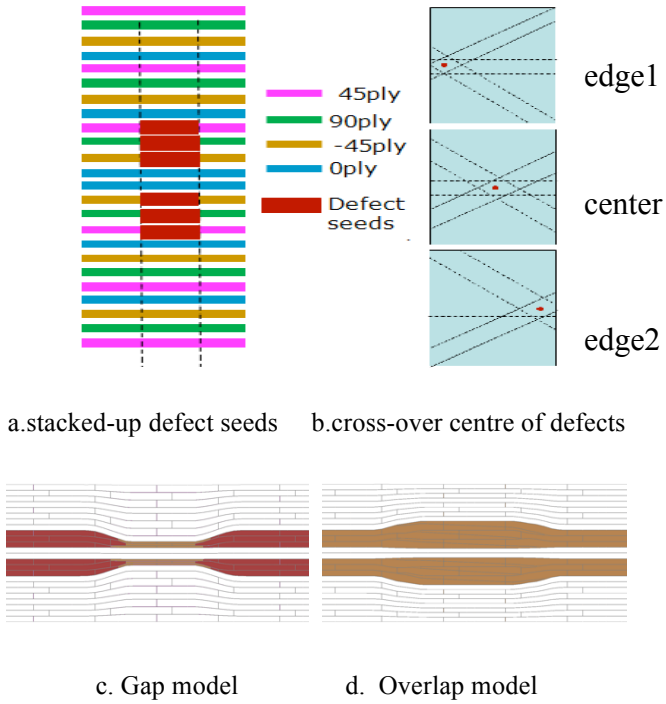

Fig.20. Stacked up defects in the inner-most plies

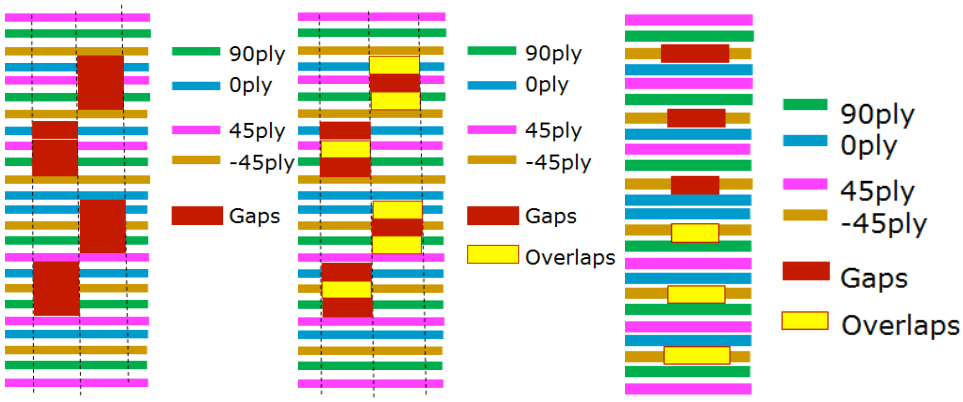

a.stacked-up gaps with stagger b.stacked-up gaps/overlaps with stagger c. coupling of gaps and overlaps

defect seeds

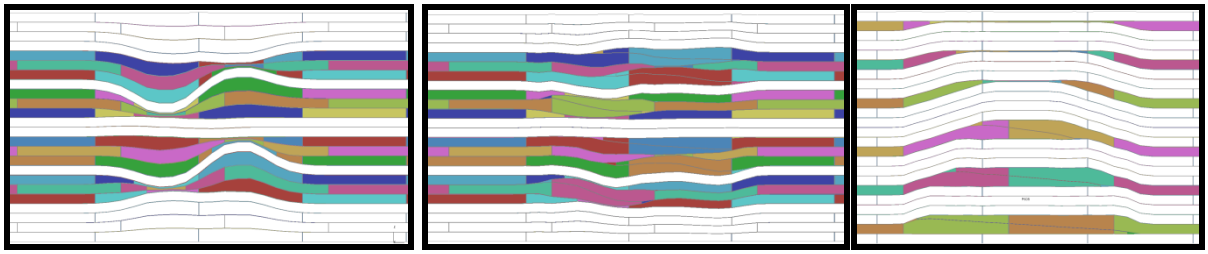

a b c

mid-plane cut section views

Fig.21 Stacked up defects with stagger and coupling of gaps and overlaps

Tables

Table 1 Fibre material properties of IM7/8552(1=fibre direction)[14]

E_{11}(GPa)	E_{22}=E_{33}(GPa)	G_{23}(GPa)	G_{12} = G_{13}(GPa)
161	11.4	3.98	5.17
$\nu_{12} = \nu_{13}$	ν_{23}	α_{11}($^{o}C^{-1}$)	α_{22}=α_{33}($^{o}C^{-1}$)
0.32	0.436	0	$3x10^{-5}$
m	σ_{unit}(MPa)		
41	3131		

Published in Science and Engineering of Composite Materials 2015; 22(2): 115–129
DOI 10.1515/secm-2013-0322

Table 2. Cohesive material properties of IM7/8552[14]

GIC (N/mm)	GIIC (N/mm)	Mode I Yield Stress (MPa)	Mode II Yield Stress (MPa)
0.2	1.0	60	90

Table 3. Comparison of tensile and compressive strength of pristine layup $[45/90/-45/0]_{3S}$ with material IM7/8552 in tests and in models

$[45/90/-45/0]_{3s}$ (IM7/8552)	Gross-Section Failure Stress(MPa)		
	Test	Model	Diff(%)
Pristine in Tension	747	740	0.94
Pristine in Compression	644	625	2.95

Delamination fibre failure